Article

Not peer-reviewed version

Presence and Variability of the Microbiome in Perivascular Adipose Tissue: A Whole-Genome Sequencing Study in Dahl SS Rats

Sameera Mahimkar , Janice Thompson , Christopher B. Blackwood , Stephanie W. Watts , Carolina B. Restini *

Posted Date: 28 February 2026

doi: 10.20944/preprints202602.2014.v1

Keywords: microbiome; perivascular adipose tissue; immune cells; whole-genome sequencing; vascular biology; Dahl SS rats

 doi:10.20944/preprints202602.2014.v1

Article

Presence and Variability of the Microbiome in Perivascular Adipose Tissue: A Whole-Genome Sequencing Study in Dahl SS Rats

Sameera Mahimkar [1], Janice Thompson [1], Christopher B. Blackwood [2] and Stephanie W. Watts [1] and Carolina B. Restini [1,*]

[1] Michigan State University, College of Osteopathic Medicine, Department of Pharmacology and Toxicology – MI, United States

[2] Michigan State University, Department of Plant, Soil, and Microbial Sciences and Department of Plant Biology – MI, United States

* Correspondence: restinic@msu.edu; Tel.: (+1) 586-263-6757; Fax: (+1) 586-416-5220

Abstract

Background. Perivascular adipose tissue (PVAT) contains adipocytes and a stromal-vascular fraction with immune cells that modulate the adjacent vasculature. The presence of immune cells in PVAT of vascular beds is poorly understood—are they resident or recruited? We propose a novel resident microbiome is present in PVAT, given the immune-rich stromal environment. **Hypothesis.** We hypothesized the existence of distinct bacterial and viral communities in healthy PVAT compared to non-PVAT adipose tissues. **Methods.** PVAT samples from thoracic and abdominal aorta, mesenteric resistance arteries, non-PVAT tissues (subscapular brown adipose tissue, retroperitoneal white adipose tissue), and fecal samples were collected one year apart from male Dahl SS rats, split into two cohorts (2023 and 2024, n=3 each). Whole-genome shotgun sequencing (CosmosID) and 16S rRNA gene analysis assessed microbial relative abundance. **Results**. PVAT harbored bacterial and viral sequences, and species composition varied significantly between cohorts. Bacterial and viral fecal samples showed lower variability. **Conclusions**. This confirms a microbiome in PVAT that differed dramatically from the fecal microbiome, with temporal influences on bacterial and viral diversity, marking the first such report. These findings establish the potential of PVAT microbiota in vascular biology and immune modulation, paving the development of microbiome-targeted drugs to address vascular dysfunctions.

Keywords: microbiome; perivascular adipose tissue; immune cells; whole-genome sequencing; vascular biology; Dahl SS rats

1. Introduction

Perivascular 1. surrounding blood vessels, such as the aorta [5–7], renal arteries [8], coronary arteries [9], and mesenteric arteries [10]. Unlike other adipose depots, PVAT is uniquely positioned in proximity to the vasculature and affects vascular function through paracrine effects that regulate vascular tone, inflammation, and remodeling [11–14].

PVAT can be grossly separated into adipocytes and a stromal vascular fraction (SVF) that is rich in immune cells. These include macrophages, T lymphocytes, and dendritic cells, which co-exist in PVAT in a healthy state [15], and may serve as a critical interface between metabolic [16] and immune processes [11]. These immune cells contribute to vascular homeostasis or pathology, depending on the physiological context [17–19]. The mechanisms governing the presence and activity of immune cells in PVAT remain unclear. Specifically, it is unclear whether immune cells in PVAT are resident populations or recruited in response to specific stimuli. Moreover, it is unclear

 doi:10.20944/preprints202602.2014.v1

whether PVATs around different arteries would have similar compositions and, yet again, differ from non-PVATs of comparable adipocyte type (e.g., brown).

An emerging area of interest is the potential role of the microbiome—encompassing bacteria, viruses, and fungi—in modulating the immune environment of PVAT. A native bacterial population has been identified within human abdominal subcutaneous, omental-visceral, and mesenteric-visceral adipose tissue [20]. The gut microbiota is well-established as a regulator of host immunity, influencing systemic inflammation and immune cell activation through microbial metabolites and direct interactions [21–23]. While the presence of microorganisms in non-gut tissues, such as adipose depots, has been documented in limited contexts (e.g., subcutaneous and visceral fat [24]), the existence and composition of a PVAT-specific microbiome remain poorly explored. Building on this paradigm, we propose that PVAT, with its immune-rich SVF, may harbor a resident microbial community that shapes its immunomodulatory functions. This gap is particularly significant given PVAT's unique anatomical and functional role in vascular health and its potential contribution to cardiovascular diseases.

The Dahl salt-sensitive (SS) rat provides an ideal model to investigate PVAT microbiome dynamics due to its relevance to cardiovascular pathology and its well-documented vascular and adipose tissue dysfunction [16,25–27]. We hypothesize that distinct bacterial and viral communities reside in the PVAT of healthy Dahl SS rats and that these microbial profiles differ from those in non-PVAT adipose tissues, such as subcutaneous or visceral fat. Furthermore, we postulate that microbiome composition varies between PVAT from conductance (thoracic and abdominal aorta) and resistance (mesenteric) vessels, reflecting their distinct physiological roles. To address these hypotheses, this study employed whole-genome sequencing (WGS) to characterize the microbiome in PVAT from aortic and mesenteric vascular beds in Dahl SS rats. It compared these profiles with those of non-PVAT adipose tissues. By identifying the presence, variability, and potential functional implications of PVAT microbial communities, this work aims to provide novel insights into the interplay between the microbiome, PVAT immunity, and vascular function, with implications for cardiovascular disease mechanisms and therapeutic strategies.

2. Methods

2.1. Animal and Sample Collection

2.1.1. Animals

All animal procedures were approved by the Michigan State University Institutional Animal Care and Use Committee (IACUC; PROTO202200001) and adhered to the *Guide for the Care and Use of Laboratory Animals* (8th edition, 2011) and ARRIVE guidelines.

Male Dahl SS rats were obtained from Charles River Laboratories (Indianapolis, IN, USA). A total of six rats (n = 6), aged 4–5 weeks at the time of arrival, were included in the study. Rats were housed under standard laboratory conditions with *ad libitum* access to water. They were fed the same standard diet (Teklad®), composed of 18.6% protein, 6.2% fat, 3.5% crude fiber, and 14.7% insoluble fiber.

Rats 1–3 were euthanized in 2023, while rats 4–6 were euthanized in 2024: **Rat 1**: Singly housed was euthanized January 9, 2023; weight at euthanasia: 450 g. **Rats 2 & 3** (housed together in one cage) were euthanized on April 4, 2023, weighing 402 g and 410 g, respectively. **Rats 4, 5** & **Rat 6** (housed together in one cage) were euthanized on February 23, 2024, weighing 421 g, 431 g, and 408 g, respectively. For tissue isolation, rats were euthanized with sodium pentobarbital (60-80 mg/kg, IP).

2.1.2. Tissue Collection

Tissue and fecal samples were collected in an aseptic environment to minimize contamination. The abdomen of the rat was swabbed with ethanol. Using sterilized surgical instruments, the following tissues were harvested: thoracic aortic perivascular adipose tissue (taPVAT), abdominal

 doi:10.20944/preprints202602.2014.v1

aortic PVAT (aaPVAT), mesenteric PVAT (mesPVAT), subscapular brown adipose tissue (BAT), retroperitoneal white adipose tissue (WAT), and feces. The fecal pellet was removed by expressing the pellet from the rectum into a sterile tube below. The fecal samples served as a positive control for the microbiome. Arterial PVATs were placed in physiological salt solution (PSS [mM]: NaCl 130; KCl 4.7; KH_2PO_4 1.18; $MgSO_4 \cdot 7H_2O$ 1.17; $NaHCO_3$ 14.8; dextrose 5.5; $CaNa_2EDTA$ 0.03, $CaCl_2$ 1.6 [pH 7.2]) for rapid dissection from the artery and placed into a sterile microcentrifuge tube.

All samples were immediately snap frozen in liquid nitrogen and stored at –80 °C until DNA extraction (**Figure 1A**). Samples were subsequently shipped on dry ice to CosmosID® for microbiome profiling via whole-genome shotgun sequencing. Samples were received by CosmosID with sufficient remaining dry ice, and samples were run blinded.

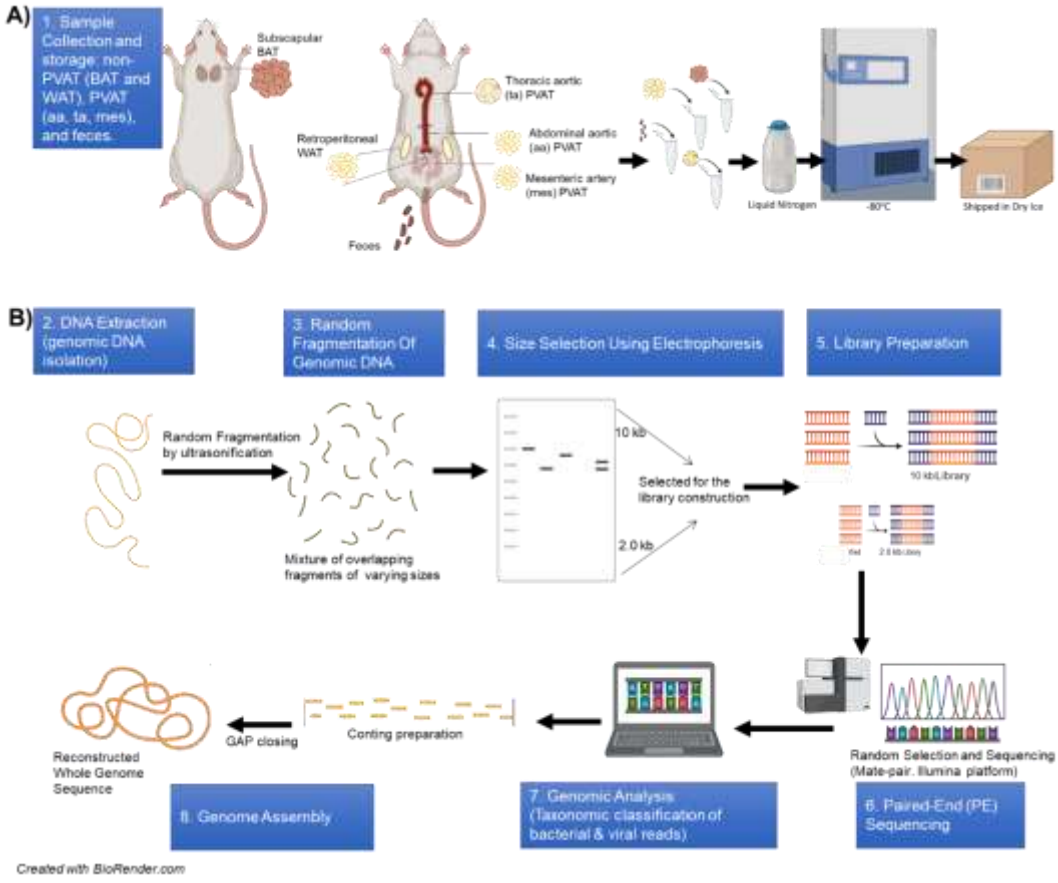

Figure 1. Schematic representation of the whole genome shotgun sequencing (WGS) laboratory and bioinformatics flow. **A)** 1. Sample collection and storage: non-PVAT (BAT: brown adipose tissue, WAT: white adipose tissue), PVAT (aa: abdominal aorta, ta: thoracic aorta, mes: mesenteric), and feces. **B)** DNA sequencing, all microbial DNA in the sample is fragmented into small pieces for next-generation sequencing: 2. isolation of genomic DNA, 3. random fragmentation of genomic DNA, 4. size selection using electrophoresis, 5. library construction, 6. paired-end sequencing (PE sequencing), 7. genomic analysis, 8. genome assembly (CosmosID Metagenomics Cloud, app.cosmosid.com, CosmosID Inc. www.cosmosid.com).

2.2. DNA Extraction and Whole Genome Sequencing

DNA extraction was performed by CosmosID® using proprietary protocols optimized for high-yield, high-quality microbial DNA isolation from low-biomass tissue and fecal samples [28]. Tissue samples were homogenized and subjected to the processes described below and depicted in **Figure 1B**. When non-proprietary in nature, protocol information was shared by CosmosID® as shown here.

 doi:10.20944/preprints202602.2014.v1

2.2.1. DNA Extraction

DNA from samples was isolated using the QIAGEN DNeasy PowerSoil Pro Kit, according to the manufacturer's protocol. Extracted DNA samples were quantified using Qubit 4 fluorometer and Qubit™ dsDNA HS Assay Kit (Thermofisher Scientific).

2.2.2. Library Preparation

DNA libraries were prepared using the Nextera XT DNA Library Preparation Kit (Illumina) and Nextera Index Kit (Illumina) with total DNA input of 1ng. Genomic DNA was fragmented using a proportional amount of Illumina Nextera XT fragmentation enzyme. Combinatory dual indexes were added to each sample followed by 12 cycles of PCR to construct libraries. DNA libraries were purified using AMpure magnetic Beads (Beckman Coulter) and eluted in QIAGEN EB buffer. DNA libraries were quantified using Qubit fluorometer and Qubit™ dsDNA HS Assay Kit. Libraries were then sequenced on an Illumina NovaSeq X platform at 2x150bp.

2.2.3. Taxonomic Profiling Methods

The system uses a high-performance k-mer data-mining algorithm that rapidly disambiguates millions of short sequence reads into discrete genomes that generate the observed sequences. The pipeline has two separable comparators: the first consists of a pre-computation phase for reference databases, and the second is a per-sample computation (CosmosID Metagenomics Cloud, app.cosmosid.com, CosmosID Inc. www.cosmosid.com). The input to the pre-computation phase was databases of reference genomes, virulence markers, and antimicrobial resistance markers that CosmosID scientists continuously curate. The output of the pre-computational phase is a phylogenetic tree of microbes, together with sets of variable-length k-mer fingerprints (biomarkers) that are uniquely associated with the tree's branches and leaves. The second per-sample computational phase searches the hundreds of millions of short sequence reads, or alternatively, contigs from draft de novo assemblies, against the fingerprint sets. This query enables the sensitive yet highly precise detection and taxonomic classification of microbial Next-Generation Sequencing (NGS) reads. The resulting statistics are analyzed to return the fine-grain taxonomic and relative abundance estimates for microbial NGS datasets. To exclude false-positive identifications, the results are filtered using a threshold derived from internal statistical scores computed from a large set of diverse metagenomes. The same approach is used to enable sensitive and accurate detection of genetic markers associated with virulence and antibiotic resistance.

2.3. Data Analysis

All six male Dahl salt-sensitive rats (rats 1–6) were initially included in the analysis. Microbiome community composition was assessed using percent relative abundance at the species level, calculated separately for bacteria and viruses, based on data generated from whole-genome shotgun sequencing of perivascular adipose tissue (PVAT) depots (ta, aa, and mes), non-PVAT adipose tissues (BAT and WAT), and fecal samples. Samples were collected at two time points separated by one year: 2023 (rats 1–3) and 2024 (rats 4–6).

Analyses were conducted in R (version 4.3.2; R Foundation for Statistical Computing, Vienna, Austria) using the "vegan" package [29] and GraphPad Prism 10.4.1 Prism. Graphs were generated using GraphPad Prism 10.4.1 and R.

2.3.1. Microbiome Community Dissimilarity Analysis and Statistics

To quantify differences in community composition and assess variability within and between sampling periods, Bray–Curtis dissimilarity was calculated from percent relative abundance values using the "vegdist" function. This metric captures compositional dissimilarity based on relative contributions of individual taxa and is commonly used for ecological and microbiome community comparisons [30].

 doi:10.20944/preprints202602.2014.v1

Pairwise Bray–Curtis distances were computed across all samples to evaluate overall community dissimilarity, as well as within individual tissue types. Bray-Curtis distances were then explored using two approaches. First, we subjected the distance matrix to principal coordinates analysis (PCoA), using the command "cmdscale", to visualize the dominant structures in the data set. Second, we used permutation-based PERMANOVA and Anderson's dispersion test [31], using the commands "adonis2" and "betadisper", respectively, to assess the significance of differences among groups. Due to limited sampling size, interactions were not formally tested (but can be assessed qualitatively in the ordinations). Using these methods, we evaluated the following questions: Do rats in different cohort years (2023, rats 1-3 vs 2024, rats 4-6) have different microbiomes? Does the microbiome of PVATs differ from that of BAT and WAT? Is the microbiome of taPVAT more similar to BAT than the other adipose tissues, or are aaPVAT and mesPVAT more similar to WAT?

2.3.2. Data Reporting

Microbial abundance data are reported as percentages of relative abundance for bacterial and viral species present at ≥1% of the total community**.** This threshold was applied to focus on biologically meaningful contributors to the microbial community and to minimize the influence of low-abundance microbial species and potential outliers that could obscure interpretation. Results are presented for each tissue type, and grouped data were used to depict relative abundance (%) across samples within each experimental cohort (1 and 2). The complete dataset, including microorganisms with relative abundances below 1% threshold, is deposited in the Supplementary Material.

3. Results:

In this section, we first present results demonstrating cohort-specific inter-individual variability across samples, as shown in the bacterial ordination (**Figure 2**) and taxon abundances (**Figure 3**), stratified by date of collection. We subsequently report the viral ordination (**Figure 4**) and the relative abundances of taxa (**Figure 5**).

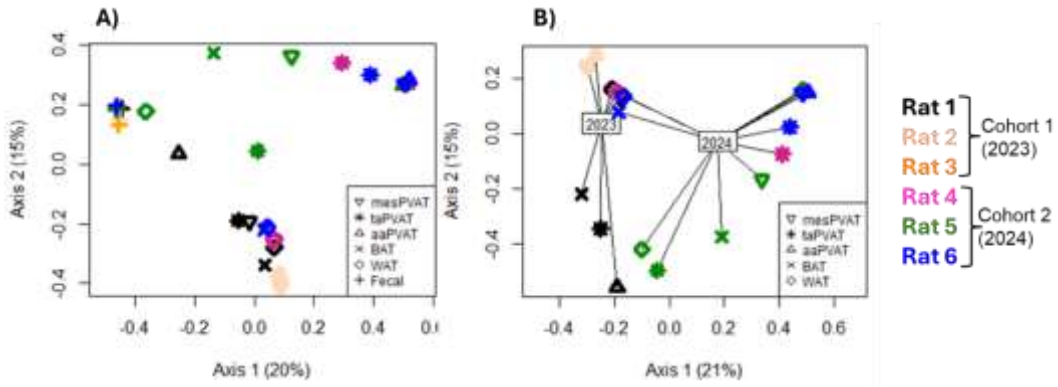

Figure 2. Bacterial community ordination using principal coordinates analysis based on Bray-Curtis distance. Rats from Cohort 1 (2023) and Cohort 2 (2024) are indicated by colors, and sample tissue types are indicated by symbol shape. Tissue types include thoracic aortic perivascular adipose tissue (taPVAT), abdominal aortic PVAT (aaPVAT), mesenteric PVAT (mesPVAT), subscapular brown adipose tissue (BAT), retroperitoneal white adipose tissue (WAT), and feces. Percents shown on axis labels indicate the proportion of variance in community composition that is summarized by that axis (i.e., the R^2 of the axis). **A)** All samples included. Fecal samples have a significantly different centroid and lower dispersion compared to other tissues ($P<0.01$). **B)** Only adipose tissues included (i.e., fecal samples excluded), with lines drawn from each sample point to the corresponding cohort centroid to illustrate the effect of year on the composition of detected bacteria ($P<0.01$).

 doi:10.20944/preprints202602.2014.v1

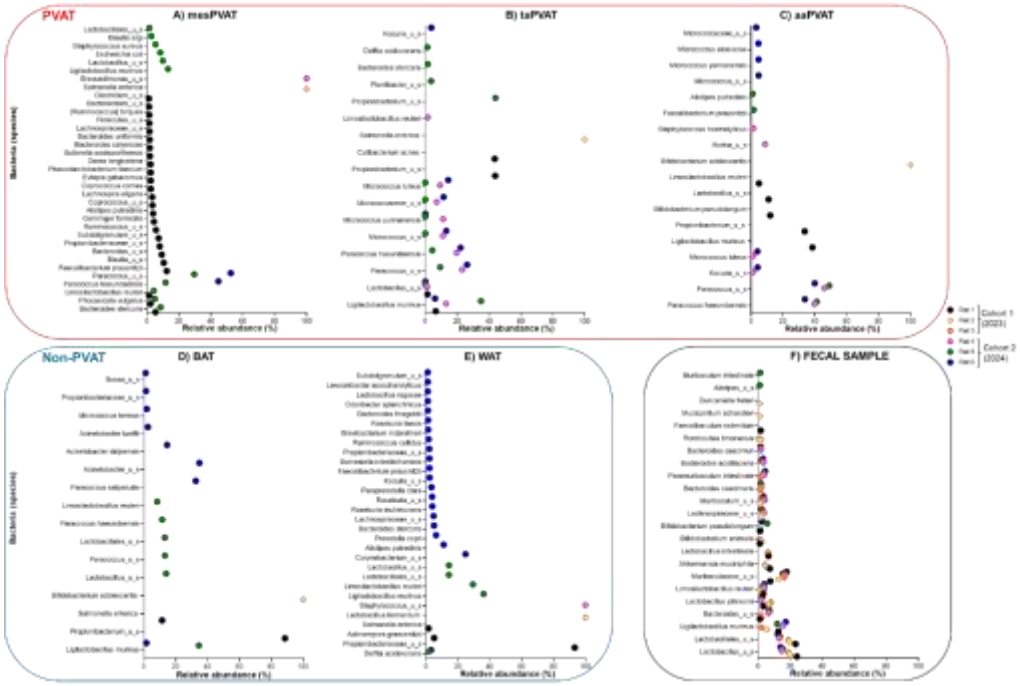

Figure 3. Relative Abundance of Diverse Bacterial Communities in PVAT and Non-PVAT Across 2023 and 2024 Cohorts. This scatter plot compares the relative abundance (%) of bacterial communities in perivascular adipose tissue (PVAT) and non-PVAT samples across Cohort 1 (2023) and Cohort 2 (2024). PVAT are shown in **A**: Mesenteric Resistance Artery (mesPVAT), **B**: Thoracic Aorta (taPVAT), and **C**: Abdominal Aorta (aaPVAT). Non-PVAT are shown in **D**: Brown Adipose Tissue (BAT) and **E**: White Adipose Tissue (WAT). Positive control is shown in **F**: Fecal Sample. The graphs display specific bacterial species (e.g., Salmonella enterica, Paracoccus spp., Lactobacillus spp.) as data points, with colors representing individual rats (Rat 1-6). The x-axis shows relative abundance, highlighting the temporal variability and diversity of bacterial communities, with PVAT exhibiting greater fluctuations than non-PVAT across the two cohorts.

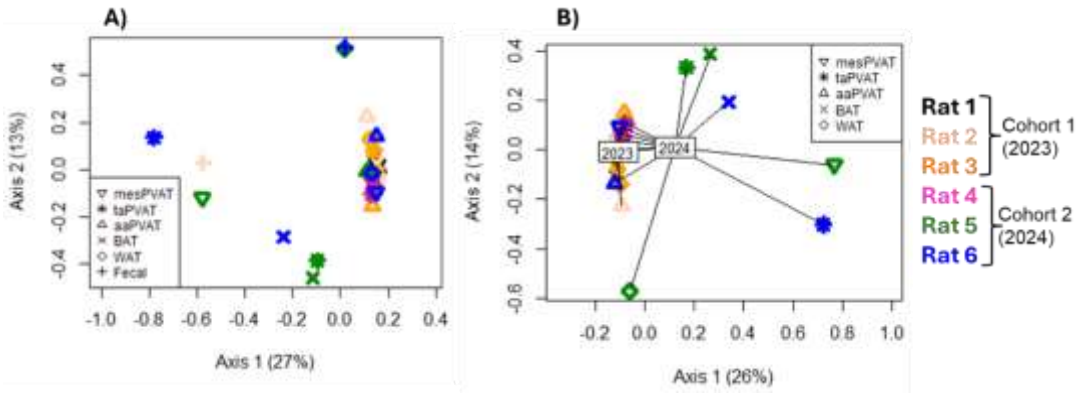

Figure 4. Viral community ordination using principal coordinates analysis based on Bray-Curtis distance. Rats from Cohort 1 (2023) and Cohort 2 (2024) are indicated by colors, and sample tissue types are indicated by symbol shape. Tissue types include thoracic aortic perivascular adipose tissue (taPVAT), abdominal aortic PVAT (aaPVAT), mesenteric PVAT (mesPVAT), subscapular brown adipose tissue (BAT), retroperitoneal white adipose tissue (WAT), and feces. Percents shown on axis labels indicate the proportion of variance in community composition that is summarized by that axis (i.e., the R^2 of the axis). **A)** All samples included. **B)** Only adipose tissues included (i.e., fecal samples excluded), with lines drawn from each point to the corresponding cohort centroid to illustrate the significant effect of year on the dispersion (variability) and composition of detected viral species ($P<0.05$).

 doi:10.20944/preprints202602.2014.v1

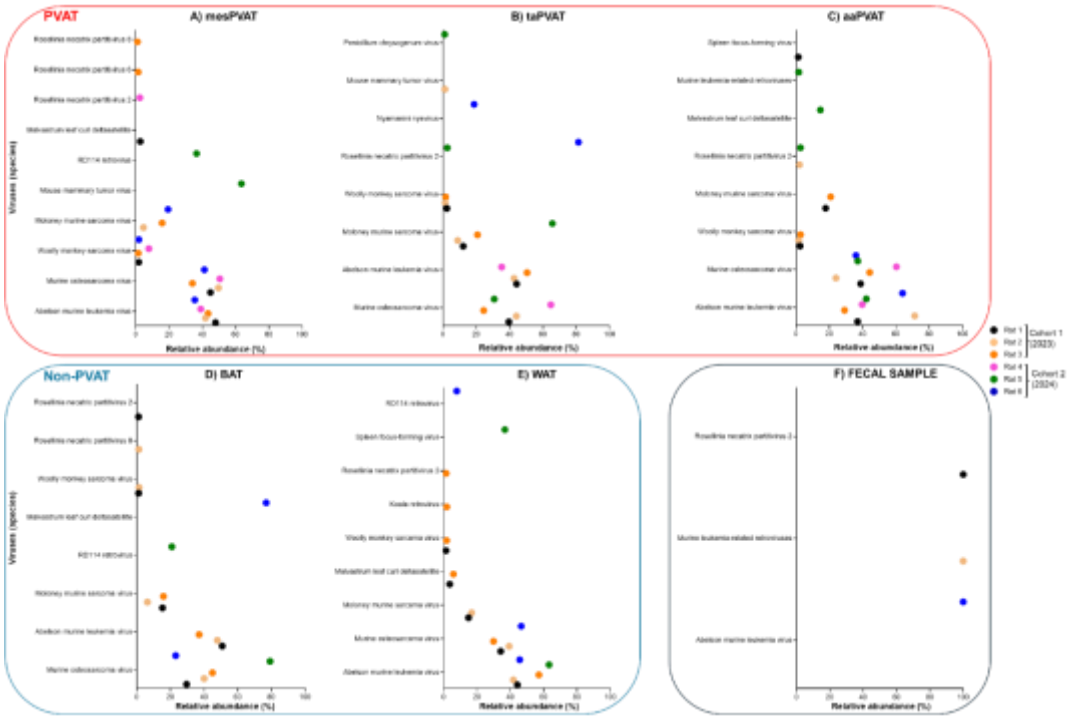

Figure 5. Viral Species Presence Across PVAT and Non-PVAT in 2023 vs. 2024 Cohorts. This scatter plot illustrates the relative abundance (%) of viral species in perivascular adipose tissue (PVAT) and non-PVAT samples across Cohort 1 (2023) and Cohort 2 (2024). PVAT are shown in **A)** Mesenteric Resistance Artery (mesPVAT), **B)** Thoracic Aorta (taPVAT), and **C)** Abdominal Aorta (aaPVAT). Non-PVAT are shown in **D)** Brown Adipose Tissue (BAT) and **E)** White Adipose Tissue (WAT). Positive control is shown in **F)** Fecal Sample. The graphs display key viral taxa (e.g., Moloney murine sarcoma virus and Abelson murine leukemia virus) as data points, with colors representing individual rats (Rat 1-6). The x-axis shows relative abundance, highlighting the consistent variability in viral species presence and abundance across both cohorts and tissue types.

3.1. Microbiome Stratification into Cohorts:

Whole-genome shotgun sequencing of DNA extracts from PVAT samples (thoracic aorta [ta], abdominal aorta [aa], and mesenteric resistance [mes] arteries), non-PVAT adipose samples that are brown (subscapular brown adipose tissue [BAT] and white (retroperitoneal adipose tissue WAT]), and fecal samples from six male Dahl SS rats revealed the presence of bacterial and viral gene sequences across all tissue types.

3.1.1. Bacterial Communities' Cohorts - Bray–Curtis Dissimilarity

The ordination of bacterial communities indicates several major patterns. First, when fecal samples are included in the ordination (**Figure 2A**), the first PCoA axis separates them from all other samples. In addition, all fecal microbiomes (from all rats and years) are clustered together (represented by the plus signs, **Figure 2A**) much more than any adipose tissue type, indicating that bacterial species composition of adipose tissue is much more variable than it is in fecal samples. Driven by the fecal samples, tissue types had significantly different centroids and dispersions ($P<0.01$, **Figure 2A**). Second, the adipose tissues (PVAT and non-PVAT) from one rat (rat 2) are tightly clustered, driven by the very low diversity in these tissues (only one bacterial species detected in each). All other rats had highly variable bacterial species composition across adipose tissue types.

After removing fecal samples (**Figure 2B**) to better focus on relationships among adipose tissue communities, there is strong separation of communities by cohort, with samples from different years mostly clustering separately along PCoA axis 1. The time frame (one year between data collections) had a significant effect on bacterial composition centroids ($P<0.01$), but not on dispersion. However,

 doi:10.20944/preprints202602.2014.v1

there is no clustering by adipose tissue type or caging history that is apparent from either ordination or permutation tests (P>0.05).

Fecal samples showed lower dispersion (variation), as indicated by the clustering of fecal points (**Figure 2A),** but also had distinct bacterial compositions, as indicated by the centroids (points representing the means of multiple axes), and greater richness of bacterial communities. Centroid differences reflect shifts in overall community composition, whereas dispersion reflects within-group variability around that composition. In other words, the fecal sample showed much less variation (**Figure 2A**), while PVAT and non-PVAT showed similar variation (**Figure 2B**).

3.1.2. Bacterial Relative Abundance and Variability of Species Across PVAT, Non-PVAT, and Fecal Samples

Below, we describe the species of bacteria with relative abundance greater than 1% in each sample (**Figure 3 A-F**). Across all samples, whole-genome shotgun sequencing identified a heterogeneous bacterial community whose composition varied by anatomical site, between cohorts, and among individual rats.

Considering PVAT depots from cohorts 1 and 2, mesPVAT, taPVAT, and aaPVAT each harbored 35, 17, and 18 distinct bacterial species in total across all rats, respectively (**Figure 3A-C)**. In non-PVAT samples, BAT showed 16 bacterial species, whereas WAT showed 30 (**Figure 3 D,E**). Fecal samples had 23 different bacterial species (**Figure 3F**).

In both PVAT and non-PVAT groups, no common bacterial species with relative abundance>1% were found across all six rats. Across adipose tissue depots, bacterial species exhibited partial, tissue-specific overlap among subsets of rats rather than universal presence, with shared taxa observed in some animals within the same cohort, in others across cohorts, and in others restricted to specific depots, highlighting pronounced inter-individual and site-dependent heterogeneity. In contrast, a core bacterial community was observed only in fecal samples, comprising seven shared species.

In the next section, to further characterize this heterogeneity, bacterial overlap patterns were examined separately within non-PVAT adipose tissues (BAT and WAT) and across individual PVAT depots (mesenteric, thoracic, and abdominal), and the shared species were described within and between cohorts.

PVAT depots

mesPVAT

Bacterial communities in mesPVAT exhibited pronounced inter-individual variability across rats and clear differences between cohorts (**Figure 3A**). In cohort 1 (2023), mesPVAT from rat 1 exhibited a diverse bacterial profile, with multiple taxa present at relative abundances above 1%. The most abundant species were *Faecalibacterium prausnitzii* (12.3%), *Blautia* _u_s. (10.5%), *Bacteroides* _u_s. (9.3%), and *Propionibacteriaceae* spp. (8.0%). Additional contributors included *Subdoligranulum* spp. (7.3%), *Ruminococcus* _u_s. (5.6%), *Bacteroides stercoris* (5.3%), *Gemmiger formicilis* (4.4%), and *Alistipes putredinis* (3.8%), with several other taxa each contributing between 1.2% and 3.4% of the community. In contrast, rat 2 mesPVAT was dominated by a single taxon, *Salmonella enterica*, which accounted for 100.0% of the detected bacterial community, while rat 3 showed no bacterial species.

In cohort 2 (2024), mesPVAT samples showed fewer dominant taxa but marked variability among animals. Rat 4 mesPVAT was exclusively composed of *Brevundimonas* _u_s (100.0%). In rat 5, the community was more diverse, with *Paracoccus* _u_s (29.6%) as the dominant taxon, followed by *Paracoccus haeu(n)daensis* (11.7%), *Ligilactobacillus murinus* (13.2%), *Lactobacillus*_u_s (9.9%), *Escherichia coli* (8.3%), *Bacteroides stercoris* (8.5%), *Staphylococcus aureus* (5.4%), *Phocaeicola vulgatus* (4.9%), *Limosilactobacillus reuteri* (4.3%), and *Blautia argi* (2.8%). Rat 6 mesPVAT was dominated by *Paracoccus* _u_s (52.5%) and *Paracoccus haeundaensis* (44.8%), with no additional taxa exceeding 1%.

Only a limited number of bacterial taxa were shared across rats, most notably mesPVAT samples collected one year apart (rats 1 and 5) shared three bacterial species: *Bacteroides stercoris, Phocaeicola vulgatus*, and *Limosilactobacillus reuteri*.

 doi:10.20944/preprints202602.2014.v1

*Paracoccus*_u_s and *Paracoccus haeundaensis* were commonly found in rats 5 and 6 (both in cohort 2)

taPVAT

taPVAT exhibited marked inter-individual variability, with distinct dominance patterns of bacterial communities across rats and between cohorts (**Figure 3B**), like findings observed in mesPVAT. In cohort 1 (2023), taPVAT from rat 1 was dominated by two closely related taxa, *Propionibacterium_u_s* (43.8%) and *Cutibacterium acnes* (43.6%), together accounting for the majority of the detected bacterial community. *Ligilactobacillus murinus* (6.5%) and *Lactobacillus_u_s* (1.4%) were also present. In contrast, taPVAT from rat 2 was composed exclusively of Salmonella enterica (100.0%), whereas rat 3 showed no bacterial species. This is the exact same pattern as in mesPVAT – no bacterial species were found in rat 3, and only Salmonella enterica in rat 2. Note that, although these two rats are grouped in the same cohort (2023), their samples were collected three months apart.

In cohort 2 (2024), taPVAT samples displayed greater taxonomic diversity but remained highly variable among animals. Rat 4 exhibited a mixed community dominated by *Paracoccus_u_s* (23.1%) and *Paracoccus haeundaensis* (19.7%), with additional contributions from *Micrococcus yunnanensis* (11.2%), *Micrococcus_u_s* (11.0%), *Micrococcus luteus* (9.2%), and *Micrococcaceae_u_s* (7.1%); *Ligilactobacillus murinus* (13.1%) and *Limosilactobacillus reuteri* (1.7%) were also detected. In rat 5, taPVAT was dominated by *Propionibacterium_u_s* (44.0%) and *Ligilactobacillus murinus* (34.9%), with smaller contributions from *Paracoccus_u_s* (9.3%), *Paracoccus haeundaensis* (4.4%), *Plantibacter_u_s* (3.7%), *Bacteroides stercoris* (1.6%), and *Delftia acidovorans* (1.3%). Rat 6 taPVAT showed dominance of *Paracoccus_u_s* (26.2%) and *Paracoccus haeundaensis* (22.1%), followed by *Micrococcus luteus* (14.4%), *Micrococcus_u_s* (13.2%), *Micrococcaceae_u_s* (11.4%), *Ligilactobacillus murinus* (6.1%), and *Kocuria_u_s* (3.7%). Four common bacterial species were found in cohort 2: *Ligilactobacillus murinus*, *Lactobacillus u_s, Paracoccus u_s,* and *Paracoccus haeundaensis.* No common bacteria were identified among the rats in cohort 1. However, one rat in cohort 1 (rat 1) and all rats in cohort 2 shared a single bacterial species (*Ligilactobacillus murinus*).

aaPVAT

Bacterial communities in aaPVAT showed substantial inter-individual variability across rats and differences between cohorts (**Figure 3C**). In cohort 1 (2023), aaPVAT from rat 1 was characterized by five taxa: *Propionibacterium_u_s* (33.6%), *Ligilactobacillus murinus* (38.5%), *Bifidobacterium pseudolongum* (12.0%), *Lactobacillus_u_s* (11.0%), and *Limosilactobacillus reuteri* (5.0%). In contrast, rat 2 aaPVAT was dominated by a single taxon, *Bifidobacterium adolescentis* (100.0%), while rat 3 showed no bacterial species. Again, this pattern repeats as observed in mesPVAT and taPVAT.

In cohort 2 (2024), aaPVAT samples displayed distinct dominance patterns across animals. Rat 4 exhibited a community dominated by *Paracoccus_u_s* (46%) and *Paracoccus haeundaensis* (39.7%), with additional taxa including *Rothia_u_s* (8.8%), *Staphylococcus haemolyticus* (1.5%), *Micrococcus luteus* (1.2%), and *Kocuria_u_s* (1.2%). aaPVAT from rat 5 was similarly dominated by *Paracoccus_u_s* (49.1%) and *Paracoccus haeundaensis* (41.2%), accompanied by *Faecalibacterium prausnitzii* (1.6%) and *Alistipes putredinis* (1.0%). In rat 6, along with the prevalence of *Paracoccus_u_s* (40.0%) and *Paracoccus haeundaensis* (33.8%), aaPVAT was also characterized by a distinct profile enriched in *Micrococcus*-associated taxa, including *Micrococcaceae_u_s* (3.2%), *Micrococcus aloeverae* (4.6%), *Micrococcus yunnanensis* (4.7%), *Micrococcus_u_s* (4.7%), and *Micrococcus luteus* (4.0%), As shown in **Figure 4C**, in aaPVAT, taxonomic overlap across animals was restricted to cohort 2, with *Paracoccus haeundaensis* and *Paracoccus*_u_s shared among rats 4–6, whereas no shared taxa were observed among the cohort 1 animals.

non-PVAT

BAT

Bacterial communities detected in subscapular BAT showed pronounced inter-individual variability in cohort 2 than in cohort 1 (**Figure 3D**). In cohort 1 (2023), BAT from rat 1 was dominated by only 2 species: *Propionibacterium_u_s* (88.6%), with *Salmonella enterica* (11.4%) comprising the remaining bacterial community above the 1% threshold. Rat 2 BAT was exclusively composed of

 doi:10.20944/preprints202602.2014.v1

Bifidobacterium adolescentis (100.0%), whereas rat 3 showed no bacterial taxa exceeding 1% relative abundance.

In cohort 2 (2024), BAT samples exhibited more diverse bacterial profiles, although dominance patterns differed in rats 5 and 6. Rat 4 showed no taxa. In contrast, rat 5 contained multiple taxa above 1%, including *Ligilactobacillus murinus* (34.5%), *Lactobacillus_u_s* (14.0%), *Lactobacillales_u_s* (13.2%), *Paracoccus_u_s* (13.2%), *Paracoccus haeundaensis* (11.5%), and *Limosilactobacillus reuteri (*8.4%). Rat 6 displayed a distinct profile dominated by *Acinetobacter_u_s* (34.9%), followed by *Paracoccus salipaludis* (32.6%), *Acinetobacter idrijaensis* (14.6%), *Acinetobacter lwoffii* (2.6%), *Micrococcus terreus* (1.9%), *Propionibacteriaceae_u_s* (1.4%), and *Bosea_u_s* (1.2%). Rats 5 and 6 shared only one bacterial species (*Ligilactobacillus murinus*); however, the percentage in rat 6 was very low compared with rat 5 (1.6% vs 34.5%).

Overall, BAT exhibited marked inter-individual variability. In cohort 1, samples were dominated by two single taxa (*Propionibacterium u_s or Bifidobacterium adolescentis), whereas cohort 2 displayed a more diverse microbial profile*, including *Ligilactobacillus murinus*, *Paracoccus* spp., *Limosilactobacillus reuteri*, and *Acinetobacter*_u_s.

WAT

Bacterial communities detected in retroperitoneal WAT comprised 30 distinct species across rats and showed clear differences between cohorts (**Figure 3E**). In cohort 1 (2023), four bacterial species were identified, whereas in cohort 2, 26 species were identified. WAT from rat 1 presented 3 species, being dominated by *Propionibacteriaceae_u_s* (93.3%), with smaller contributions from *Actinomyces graevenitzii* (5.1%) and *Salmonella enterica* (1.6%). In contrast, rat 2 WAT was exclusively composed of one species (*Lactobacillus fermentum*), while rat 3 showed no bacteria. It is remarkable that this pattern is exactly that of BAT and all PVAT samples (i.e., no bacterial species in rat 3 and only one in rat 2).

In cohort 2 (2024), WAT samples exhibited distinct dominance patterns across animals, with the majority of species found in rat 6 (21 distinct bacterial species). In rat 6, WAT exhibited the highest taxonomic diversity, with multiple taxa present above 1%, including *Corynebacterium_u_s* (24.8%), *Alistipes putredinis* (11.1%), *Prevotella copri* (6.3%), *Bacteroides stercoris* (5.0%), *Lachnospiraceae_u_s* (4.8%), *Roseburia inulinivorans* (4.0%), *Roseburia_u_s* (3.9%), *Paraprevotella clara* (3.5%), *Kocuria_u_s* (2.3%), *Faecalibacterium prausnitzi*i (2.2%), *Barnesiella intestinihominis* (2.2%), *Propionibacteriaceae_u_s* (2.1%), *Ruminococcus callidus* (1.7%), *Delftia acidovorans* (3.2%), and several additional taxa each contributing between 1.1% and 1.4%. Rat 5 displayed a moderate heterogeneous bacterial profile, with *Ligilactobacillus murinus* (36.1%) as the most abundant taxon, followed by *Limosilactobacillus reuteri (*29.5%), *Lactobacillus_u_s* (14.4%), *Lactobacillales_u_s* (14.4%), and *Delftia acidovorans* (1.7%). Rat 4 WAT was exclusively dominated by *Staphylococcus_u_s* (100.0%).

Fecal Sample

Fecal bacterial communities exhibited relatively consistent profiles across rats, with multiple taxa contributing moderate relative abundances in both cohorts (**Figure 3F**).

Fecal microbiota displayed relatively consistent community structures across both cohorts, dominated by *Lactobacillus_u_s, Lactobacillales_u_s, Muribaculaceae_u_s, and Ligilactobacillus murinus (ranging from 2.4–24.2%),* with cohort-specific differences observed in lower-abundance taxa.

In cohort 1 (2023), fecal samples from rats 1, 2, and 3 were dominated by *Lactobacillus_u_s* (24.2, 20, 19.1%, respectively) *and Lactobacillales_u_s (23.4, 19.5, 18.8%*, respectively*),* together accounting for a substantial proportion of the bacterial community. *Muribaculaceae_u_s* was also shared across all three rats (16.2, 12.7,7.61%, respectively), along with *Ligilactobacillus murinus* (12.6, 5.4, 2.4%, respectively), *Akkermansia muciniphila* (7.3, 5.0 ,4.3%, respectively), *Lactobacillus intestinalis* (6.4, 6.5, 6.2%, respectively), *Lactobacillus johnsonii* (3.2, 5.8, 7.8%, respectively), *Limosilactobacillus reuteri* (3.2, 1.4, 1.2%, respectively), and *Bacteroides_u_s* (1.1, 2.2, 1.6%, respectively) and *Bifidobacterium animalis* (1.0, 2.6, 1.3%, respectively). *Bifidobacterium pseudolongum* was present in rats 1 and 2 (1.2, 1.3, respectively), but not in rat 3; where as *Lachnospiraceae_u_s and Romboutsia timonensis were identified in rats 2 and 3 but not rat 1:* 1.7% (rat 2), 2.7% (rat 3), respectively and 1.2% (rat 2) 1.6% (rat 3), respectively.

 doi:10.20944/preprints202602.2014.v1

In cohort 2 (2024), with rats 4, 5, and 6, fecal profiles were similarly structured, with *Lactobacillus_u_s (14.8, 15.4, 14.0%) and Lactobacillales_u_s (13.2, 13.5, 12.3%). Muribaculaceae_u_s again* represented a major component of the community (16.7, 15.4, 17.8%), alongside *Ligilactobacillus murinus* (15.5, 11.9, 17.2%). Additional taxa present above the 1% threshold included *Bacteroides_u_s* (6.4, 7.0, 6.7%), *Muribaculum_u_s* (4.2, 2.6, 3.3%), *Paramuribaculum intestinale* (3.5, 3.5, 4.3%), *Bacteroides acidifaciens* (3.3, 2.2, 3.0%), *Lactobacillus johnsonii* (1.8, 1.8 2.5%), *Limosilactobacillus reuteri* (3.7, 2.8, 3.7%), *and Lachnospiraceae_u_s* (3.5, 3.1, 1.9%). *In contrast to cohort 1, Akkermansia muciniphila* and *Lactobacillus intestinalis* were not detected at> 1% in fecal samples from cohort 2.

Across fecal samples, seven bacterial taxa were consistently detected in all rats from both cohorts at relative abundances exceeding 1%, including *Lactobacillus_u_s*, *Lactobacillales_u_s*, *Ligilactobacillus murinus*, *Bacteroides_u_s*, *Lactobacillus johnsonii*, *Limosilactobacillus reuteri*, and *Muribaculaceae_u_s*, each contributing moderate relative abundances across animals.

Although fecal samples exhibited the greatest number of bacterial taxa shared across all rats and both cohorts—a pattern not observed in PVAT or non-PVAT adipose tissues—the maximum relative abundance of any single fecal taxon was modest, reaching 24.2%, which was substantially lower than the dominant taxa observed in PVAT depots (mesPVAT, taPVAT, aaPVAT) and non-PVAT adipose tissues (BAT and WAT).

3.1.3. Viral Communities' Cohorts - Bray–Curtis Dissimilarity

Ordination of viral communities did not reveal clustering by any tissue type, including feces, compared to PVAT and non-PVAT adipose tissues (**Figure 4A**; P>0.05).

Fecal viral communities were characterized by extreme inter-individual specificity, with dominance of a single viral taxon when present and complete absence of ≥1% viruses in several animals. Notably, fecal samples from Rat 4 did not detect any viral species ≥1%, consistent with the absence observed in BAT and WAT from the same animal.

Interestingly, BAT, WAT, and fecal samples from Rat 4 didn't detect any viral species.

Rats in cohort 2 were housed together and exhibited a highly diverse viral profile across samples. After removing fecal samples, the strong impact of cohort became apparent (**Figure 4B**). Year had a significant effect on both viral composition centroids and dispersion (P<0.01), with 2024 samples showing much greater composition variance than 2023 samples. Viral species relative-abundance profiles differed between rats 1–3, exhibiting more consistent tissue-specific compositions than rats 4–6, which, overall, showed greater inter- and intra-individual variability (**Figure 4A-B**).

3.1.4. Viral Relative Abundance and Variability of Species Across PVAT, Non-PVAT, and Fecal Samples

Considering PVAT depots from cohorts 1 and 2, mesPVAT, taPVAT, and aaPVAT each harbored 17, 15, and 13 distinct virus species, respectively, across all rats sampled (**Figure 5A-C**). Among PVAT depots, mesPVAT, aaPVAT, and taPVAT shared 8 virus species (*Abelson murine leukemia virus, Moloney murine sarcoma virus, Murine leukemia-related retroviruses, Murine osteosarcoma virus, Penicillium chrysogenum virus, RD114 retrovirus, Rosellinia necatrix partitivirus 2,* and *Woolly monkey sarcoma virus*).

In non-PVAT samples, BAT and WAT showed a similar amount of species (15 and 14, respectively) (**Figure 5 D,E**), sharing with 9 virus species (*Abelson murine leukemia virus, Malvastrum leaf curl deltasatellite, Feline leukemia virus, Moloney murine sarcoma virus, Murine osteosarcoma virus, Penicillium chrysogenum virus, RD114 retrovirus, Rosellinia necatrix partitivirus 2* and *Woolly monkey sarcoma virus*).

Across adipose compartments, there are overlapping viral profiles between vascular-associated and non-vascular adipose compartments. PVAT depots (mesPVAT, aaPVAT, and taPVAT) and non-PVAT tissues (BAT and WAT) shared 7 virus species (*Abelson murine leukemia virus, Malvastrum leaf curl deltasatellite, Feline leukemia virus, Moloney murine sarcoma virus, Murine osteosarcoma virus, Rosellinia necatrix partitivirus 2,* and *Woolly monkey sarcoma virus*). In contrast, fecal samples exhibited

 doi:10.20944/preprints202602.2014.v1

a profoundly limited viral repertoire, with only three virus species detected, all of which were also present in non-PVAT adipose tissues and overlapped with PVAT depots (**Figure 5F**).

Below, we describe the results, by cohort, of viral species relative abundance above the 1% threshold across tissues, as depicted in **Figure 5 (A-F**).

PVAT Depots

Across all PVAT depots, viral communities were dominated by murine retroviruses, primarily *Abelson murine leukemia virus* and *murine osteosarcoma virus* (**Figure 5A–C**). However, these communities exhibited depot- and cohort-specific patterns of inter-individual variability.

In cohort 1 (rats 1–3; 2023), mesPVAT, taPVAT, and aaPVAT consistently displayed profiles dominated by these two retroviruses, frequently accompanied by *Moloney murine sarcoma virus* at intermediate relative abundance, with occasional additional species exceeding 1% in individual animals (e.g., Woolly *monkey sarcoma* virus or *Rosellinia necatrix* partitivirus species).

In cohort 2 (rats 4–6; 2024), PVAT viral composition was more heterogeneous across depots and individuals. While some rats retained retrovirus-dominant profiles comparable to cohort 1 (e.g., rats 4 and 6 in mesPVAT and aaPVAT), others exhibited distinct compositions, including dominance of mouse mammary tumor virus and *RD114 retrovirus* in mesPVAT (rat 5), enrichment of *Moloney murine sarcoma virus* or *Rosellinia necatrix* partitivirus 2 in taPVAT (rats 5 and 6, respectively), and broader intermediate-abundance profiles in aaPVAT driven by additional species in select animals. Overall, PVAT from cohort 2 shows variability within the same rat across tissue samples (mes, ta, and aa) and across rats within the same tissue. Collectively, these findings indicate that, although a core retroviral signature characterizes PVAT across depots, cohort 2 exhibits greater inter- and intra-individual variability than cohort 1.

mesPVAT

Viral communities detected in mesPVAT exhibited pronounced inter-individual variability across rats and differences between cohorts (**Figure 5A**). In mesPVAT, all rats from cohort 1 (rats 1–3) and two rats from cohort 2 (rats 4 and 6) exceeded the 1% relative abundance threshold for Abelson murine leukemia virus and Murine osteosarcoma virus.

In cohort 1 (2023), mesPVAT from rats 1–3 was dominated by *Abelson murine leukemia virus* (47.9, 41.9, 43.1%) and *Murine osteosarcoma virus* (44.9, 59.7, 34.1%), which together accounted for the majority of viral relative abundance in all three animals. Additional viral species detected above the 1% threshold in cohort 1 included *Woolly monkey sarcoma virus* in rats 1 and 2 (1.8 and 1.5%, respectively) and *Moloney murine sarcoma virus* in rats 2 and 3 (4.7 and 15.9%, respectively). Lower-abundance viruses present in individual animals included *Malvastrum leaf curl deltasatellite* (2.7% in rat 1), *Rosellinia necatrix partitivirus 6* (1.4% in rat 3), and *Rosellinia necatrix partitivirus 8* (1.0% in rat 3).

In cohort 2 (2024), mesPVAT viral profiles differed markedly across animals. Rat 4 showed dominance by Murine osteosarcoma virus (50.5%) and *Abelson murine leukemia virus* (39.1%), with *Woolly monkey sarcoma virus* accounting for an additional 7.9%. In contrast, rat 5 exhibited a distinct viral profile dominated by *Mouse mammary tumor virus* (63.5%) and *RD114 retrovirus* (36.5%), with no other viral species exceeding the 1% threshold. Rat 6 mesPVAT again showed high relative abundances of *Abelson murine leukemia virus* (35.5%) and *Murine osteosarcoma virus* (41.3%), with *Moloney murine sarcoma virus* (19.4%) and *Woolly monkey sarcoma virus* (1.9%) also detected.

In summary, mesPVAT viral communities were dominated by a small number of retroviruses, with *Abelson murine leukemia virus* and *Murine osteosarcoma virus* accounting for the majority of relative abundance in most animals, while distinct cohort-specific dominance patterns were observed in individual rats.

taPVAT

In PVAT from the thoracic aorta, perivascular adipose tissue (taPVAT), we found marked inter-individual variability across rats and differences between cohorts (**Figure 5B**). In cohort 1 (2023), taPVAT from rats 1–3 was dominated by *Abelson murine leukemia virus* (44.2, 42.6, 50.5%) and *Murine osteosarcoma virus* (39.5, 44.0, 24.4%), which together accounted for the majority of viral relative abundance in all three animals. *Moloney murine sarcoma virus* was also consistently detected in cohort

 doi:10.20944/preprints202602.2014.v1

1, contributing 12.1% in rat 1, 8.8% in rat 2, and 20.7% in rat 3. Lower-abundance viral species present above the 1% threshold included *Woolly monkey sarcoma virus* (2.3, 1.3, 1.6%) across all three rats and *Mouse mammary tumor virus* (1.1% in rat 2).

In cohort 2 (2024), taPVAT viral profiles diverged substantially between animals. Rat 4 exhibited strong dominance *of Murine osteosarcoma virus* (64.7%) and *Abelson murine leukemia virus* (35.3%), with no additional viral species exceeding 1%. In contrast, rat 5 showed a distinct profile dominated by *Moloney murine sarcoma virus* (65.7%) and *Murine osteosarcoma virus* (30.8%), accompanied by *Rosellinia necatrix partitivirus 2* (2.5%). Rat 6 taPVAT was characterized by a high relative abundance of *Rosellinia necatrix partitivirus 2* (81.4%) and *Nyamanini nyavirus* (18.6%), with no other viral species detected above the 1% threshold. taPVAT viral communities were dominated by a small number of viral species, with *Abelson murine leukemia virus* and *Murine osteosarcoma virus* prevalent in cohort 1, whereas in cohort 2, taPVAT viral profiles differed markedly between animals, with rat 4 dominated by murine retroviruses, rat 5 dominated by *Moloney murine sarcoma virus*, and rat 6 dominated by *Rosellinia necatrix partitivirus 2*. *Murine osteosarcoma virus* was detected in all rats from both cohorts except rat 6 (cohort 2), indicating its widespread presence across animals despite inter-individual variability in viral dominance patterns.

aaPVAT

Viral communities detected in abdominal aorta perivascular adipose tissue (aaPVAT) were dominated by a small number of viral species across rats, with differences in relative abundance observed between cohorts (Figure 5C). In cohort 1 (2023), aaPVAT from rats 1–3 was consistently dominated by *Abelson murine leukemia virus* (37.0, 71.3, 29.1%) and *Murine osteosarcoma virus* (38.8, 23.9, 44.2%). Additional viral species detected in cohort 1 included *Moloney murine sarcoma virus* (17.8% in rat 1 and 20.8% in rat 3) and *Woolly monkey sarcoma virus* (2.5, 1.7, 2.7%). *Spleen focus-forming virus* was detected at 1.4% in rat 1 only.

In cohort 2 (2024), aaPVAT viral profiles remained dominated by the same two retroviruses but with notable inter-individual variability. Rats 4–6 showed high relative abundances of *Murine osteosarcoma virus* (60.3, 37.1, 36.0%) and *Abelson murine leukemia virus* (39.7, 42.2, 64.0%). Additional viral species above 1% were detected selectively, including *Rosellinia necatrix partitivirus 2* (2.7% in rat 5), *Malvastrum leaf curl deltasatellite* (14.6% in rat 5), and *Murine leukemia-related retroviruses* (1.7% in rat 5). No other viral taxa exceeded the 1% threshold in cohort 2 aaPVAT samples.

Remarkably, in aaPVAT two viral communities were consistently dominated across both cohorts: *Abelson murine leukemia virus* and *Murine osteosarcoma virus*, with reasonably high relative abundance (> 24%).

Non-PVAT

BAT

Viral communities detected BAT displayed marked inter-individual variability and distinct patterns between cohorts (**Figure 5D**). In cohort 1 (2023), BAT samples from rats 1–3 were dominated by *Abelson murine leukemia virus* (50.8, 47.9, 37.0%), *Murine osteosarcoma virus* (29.6, 40.0, 44.9%), and *Moloney murine sarcoma virus* (15.2, 6.3, 15.8%). Lower-abundance viral species detected above the 1% threshold included *Woolly monkey sarcoma virus* (1.1, 1.3, 0%) and *Rosellinia necatrix partitivirus 2* (1.0% in rat 1).

In cohort 2 (2024), BAT viral profiles differed substantially across animals. Rat 4 showed no viral species. In contrast, rat 5 BAT was dominated by *Murine osteosarcoma virus* (79.2%), with *RD114 retrovirus* contributing an additional 20.8%. Rat 6 exhibited a distinct profile characterized by strong dominance of *Malvastrum leaf curl deltasatellite* (76.9%), accompanied by *Murine osteosarcoma virus* (23.1%). No other viral taxa exceeded the 1% threshold in cohort 2 BAT samples. With the exception of rat 4 (cohort 2), *the Murine osteosarcoma virus was detected* in BAT samples from all rats across both cohorts.

Overall, BAT viral communities were dominated by murine retroviruses in cohort 1, whereas cohort 2 exhibited pronounced inter-animal divergence, including single-virus dominance by *Murine osteosarcoma virus* or *Malvastrum leaf curl delta satellite.*

 doi:10.20944/preprints202602.2014.v1

WAT

Viral communities detected in WAT (retroperitoneal) showed substantial inter-individual variability across rats and clear differences between cohorts (**Figure 5E**). In cohort 1 (2023), WAT samples from rats 1–3 were consistently dominated by *Abelson murine leukemia virus* (44.2, 41.9, 57.1%) and *Murine osteosarcoma virus* (34.2, 39.3, 29.9%). *Moloney murine sarcoma virus* was also present above the 1% threshold in rats 1 and 2, contributing 14.9% and 16.8%, respectively. Additional viral species detected above 1% in individual animals included *Malvastrum leaf curl deltasatellite* (3.6% in rat 1 and 5.8% in rat 3), *Woolly monkey sarcoma virus* (1.4,0, 1.7%), *Koala retrovirus* (1.8% in rat 3), and *Rosellinia necatrix partitivirus 2* (1.4% in rat 3).

In cohort 2 (2024), WAT viral profiles diverged markedly between animals. Rat 4 showed no viral species exceeding the 1% relative abundance threshold. In contrast, rat 5 WAT was dominated by *Abelson murine leukemia virus* (63.3%), accompanied by *Spleen focus-forming virus* (36.7%). Rat 6 displayed a distinct profile characterized by high relative abundances of *Abelson murine leukemia virus* (45.6%) and *Murine osteosarcoma virus* (46.5%), with *RD114 retrovirus* contributing an additional 7.8%.

In WAT, *Abelson murine leukemia virus* was detected in all rats from both cohorts except rat 4 (cohort 2), which, as observed in BAT, showed no viral species. In contrast, *Murine osteosarcoma virus* was detected in all rats in cohort 1 (rats 1–3) and in rat 6 in cohort 2, but was not detected in the remaining cohort 2 animals.

Fecal Samples

Fecal viral communities were sparse and highly individualized, with single-virus dominance observed in isolated animals and no viral species shared across rats or cohorts (**Figure 5F**). In fecal samples, only three virus species were found in total. These were limited to three animals: rats 1 and 2 (both Cohort 1, 2023), which harbored *Rosellinia necatrix partitivirus* 2 and *Murine leukemia-related retroviruses*, respectively, while rat 6 (Cohort 2, 2024) was the only one harboring *Abelson murine leukemia virus*. No viral species were detected in fecal samples from any of the other animals, indicating that detectable fecal viral profiles were sparse and highly individualized across cohorts and independent of collection time points (**Figure 5F**). Notably, among the three viruses identified in fecal samples, *Rosellinia necatrix partitivirus 2* and *Abelson murine leukemia virus* were detected above the 1% relative abundance threshold in both all PVAT (Figure 5A-C) and non-PVAT (**Figure 5D-E**) samples. In contrast, *Murine leukemia-related retroviruses* were found only in aaPVAT (**Figure 5C**).

In contrast to bacterial communities, no viral taxa were shared across all tissue types when fecal samples were included. However, several murine retroviruses—most notably *Abelson murine leukemia virus* and *Murine osteosarcoma virus*—were consistently detected across all PVAT depots and non-PVAT adipose tissues, with fecal viral profiles showing sparse, animal-specific dominance patterns.

4. Discussion

We presently describe the use of metagenomic sequencing to characterize bacterial and viral communities within PVATs and non-PVATs of healthy male Dahl SS rats, as compared to the standard of fecal microbiome burden. Our findings demonstrate the presence of PVAT microbiomes and reveal temporal variability in their bacterial and viral composition. To our knowledge, this is the first study to provide direct evidence of bacterial and viral communities in PVAT surrounding both conductance and resistance vessels.

Do mes, aa, and taPVAT samples collected one year apart present different microbiomes?

Yes. Cohort year was associated with significant differences in both bacterial (**Figure 2**) and viral community composition (**Figure 4**), with stronger effects observed in viral communities. Viral profiles exhibited both centroid shifts and increased dispersion in 2024, indicating greater inter-individual heterogeneity compared to 2023 (**Figure 4B**). In contrast, bacterial communities showed significant centroid separation by cohort without significant dispersion differences after removal of fecal samples (**Figure 2B**). This pattern suggests that bacterial differences were structured compositional shifts between years, whereas viral differences reflected both compositional change

 doi:10.20944/preprints202602.2014.v1

and increased variability. Together, these findings indicate that temporal factors exert a substantial influence on adipose-associated microbial signatures, particularly within the virome.

Importantly, adipose depot identity did not significantly structure either bacterial or viral communities. No clustering was observed by PVAT subtype (mes, ta, aa) or by non-PVAT adipose depots (BAT, WAT), and no preferential similarity was detected between thoracic PVAT and BAT or between abdominal/mesenteric PVAT and WAT. Thus, temporal stratification exceeded anatomical depot effects in shaping the adipose-associated microbiome.

In bacterial analyses, cohort year was associated with a significant shift in community centroids without differences in dispersion, indicating a consistent compositional restructuring between 2023 and 2024. In contrast, viral communities demonstrated both centroid shifts and increased dispersion in 2024, suggesting greater inter- and intra-individual heterogeneity of the virome relative to the bacteriome. Within individual depots, aaPVAT exhibited relatively consistent cohort-specific patterns; however, this did not translate into overall depot-driven clustering across the dataset. Bacterial communities in cohort 2 aaPVAT were characterized by reproducible dominance of *Paracoccus* spp. (**Figure 3C**), while viral communities in cohort 1 aaPVAT were uniformly dominated by murine retroviruses (**Figure 5C**). In contrast, cohort 1 bacterial profiles in PVAT were highly heterogeneous, whereas viral profiles in the same cohort were comparatively conserved.

Does PVAT differ from BAT and WAT?

The data we share do not support PVATs (white or brown) being different in their microbiome family from WAT and BAT, respectively. Although for different reasons, neither viral nor bacterial PVAT presented differences from non-PVAT depots. In bacterial species, the absence of separation, as evidenced by the lack of clustering by adipose tissue type, indicated no significant differences in bacterial community structure. Ordination of viral communities did not reveal clustering by any tissue type, indicating no separation between PVAT vs BAT vs WAT, nor between fecal vs adipose depots, unlike bacteria.

Is taPVAT more similar to BAT? Or aaPVAT/mesPVAT more similar to WAT?

The PVAT phenotype is dependent on its anatomical location, with taPVAT exhibiting a brown PVAT signature, while aaPVAT shows a WAT-like phenotype [32]. We raised the question of whether the microbiome of taPVAT would be more similar to BAT than to the other adipose tissues, or whether aaPVAT and mesPVAT would be more similar to WAT. We found no evidence of structured similarity in either viral or bacterial communities, with no adipose tissue-type clustering, as indicated by the lack of tissue-level clustering and by the absence of tissue-type effects in permutation tests.

The PVAT phenotype varies by anatomical location: thoracic PVAT exhibits a brown-like signature, whereas abdominal PVAT displays a WAT-like phenotype (Ahmadieh et al., 2020). We therefore tested whether microbial community structure paralleled this adipose identity—that is, whether taPVAT would more closely resemble BAT and whether aaPVAT or mesPVAT would align more closely with WAT. Importantly, although cohort-specific patterns were observable within individual depots, including aaPVAT (as describe above), these reflected temporal structuring rather than depot-driven microbial specialization. Neither bacterial nor viral datasets demonstrated clustering consistent with brown-versus-white adipose phenotype.

For bacteria, these results indicate that temporal cohort effects, rather than adipose depot identity, were the dominant driver of bacterial community structure. For viruses: as for bacteria, viral communities were structured primarily by cohort year; however, unlike bacteria, viral communities in 2024 also exhibited significantly greater dispersion, indicating increased heterogeneity.

Overall, temporal stratification dominates microbiome structure; tissue type does not structure microbial communities; viral communities are more temporally unstable than bacterial communities, and fecal bacterial communities are highly conserved and distinct.

Inter-cohort temporal effects exceed anatomical depot effects in shaping adipose-associated microbiome structure.

Bacterial Community Patterns Across Depots

 doi:10.20944/preprints202602.2014.v1

Across PVAT, non-PVAT adipose tissues, and feces, only three bacterial taxa exceeded the 1% relative abundance threshold in all tissue types: *Lactobacillus (unclassified species)*, *Ligilactobacillus murinus*, and *Limosilactobacillus reuteri*. Although these taxa were detectable across compartments, their relative abundances varied substantially by tissue and by animal, indicating that cross-tissue presence does not imply uniform representation. In contrast to adipose tissues, fecal samples exhibited a broader shared core across animals and cohorts, highlighting the distinct ecological structure of adipose-associated bacterial communities.

These findings suggest that adipose-associated bacterial communities—particularly within PVAT—are not simple reflections of fecal microbiota but instead represent selective, tissue-associated profiles characterized by limited overlap and substantial inter-animal variability. Importantly, the wide range of relative abundances observed for those shared taxa across tissues further emphasizes that cross-tissue presence does not imply uniform dominance, underscoring the need to consider both prevalence and relative abundance when interpreting microbial signatures across anatomical niches.

Viral Community Structure and Restricted Overlap

In contrast to bacterial communities, viral profiles exhibited a markedly more restricted overlap across tissues, with no viral taxa detected above the 1% relative abundance threshold across all sampled tissue types when fecal samples were included (**Figure 5A-F**).

Within adipose tissues, seven viral taxa were detected in both PVAT and non-PVAT depots, including multiple murine retrovirus reference genomes (e.g., Abelson murine leukemia virus, Moloney murine sarcoma virus, Woolly monkey sarcoma virus, and Murine osteosarcoma virus), as well as non-mammalian viral references. Viral communities were characterized by dominance of a small number of taxa and pronounced variability in relative abundance across animals and cohorts. Fecal viral communities were sparse and highly individualized, often dominated by a single virus in isolated animals. Collectively, these patterns indicate that viral detection across adipose tissues reflects restricted, heterogeneous sequence signatures rather than a uniform, broadly distributed virome. The observed inter-individual variability appears largely driven by the disproportionate dominance of distinct viral taxa within specific animals. Because endogenous retroviral elements are pervasive within mammalian genomes and can be transcribed, and because low-biomass metagenomic datasets are susceptible to reagent and laboratory background contamination, shared retroviral detections should be interpreted as overlapping sequence signatures rather than definitive evidence of compartment-specific productive infection [33].

Environmental and Housing Considerations

Environmental context may have contributed to the observed cohort stratification. Rats in cohort 2 were group-housed together, whereas cohort 1 included both single- and co-housed animals. Housing conditions are known to influence microbial exchange in rodents [34] and could partially contribute to between-cohort structuring. However, all animals were maintained on the same chow formulation, and similarities observed across individual animals from different cohorts argue against a purely cage-driven effect. Although the present study was not powered to formally disentangle housing from temporal effects, the consistent cohort-level separation across both bacterial and viral datasets suggests that year-associated environmental or colony-level factors likely exert stronger influence than adipose depot identity in this model.

PVAT as a Distinct Microbial Microenvironment

Across both bacterial and viral communities, PVAT exhibited pronounced cohort-specific signatures, whereas non-PVAT adipose depots showed greater inter-animal variability. Overall temporal cohort emerged as the dominant organizing factor of microbiome structure, whereas adipose depot identity did not significantly structure community composition.

Notably, neither bacterial nor viral profiles clustered by adipose tissue subtype (PVAT vs. BAT vs. WAT), and no evidence supported preferential similarity of thoracic PVAT to BAT or of abdominal/mesenteric PVAT to WAT.

Our detection of diverse bacterial genera, such as *Paracoccus*, *Salmonella*, *Lactobacillus*, and *Ligilactobacillus*, in PVAT aligns with emerging reports on microbiota in adipose depots (Patel et al.,

 doi:10.20944/preprints202602.2014.v1

2022; Queiroz & Sena, 2024; Zhang et al., 2025). Prior work has largely focused on indirect gut–PVAT interactions mediated by circulating metabolites (e.g., TMAO[39,40] in models of metabolic disease, focused on the indirect effects of gut microbiota on PVAT function rather than the resident communities [41]. Our findings suggest that adipose tissues themselves harbor detectable microbial signatures beyond the gut, though their biological relevance remains to be determined.

The cohort-specific bacterial variability observed in the present study could reflect environmental or temporal factors, such as subtle changes in animal housing or microbial drift over time. This temporal instability in bacteria contrasts with the consistency of viral taxa, such as *Abelson murine leukemia virus* and *Moloney murine sarcoma virus*, potentially indicating that viruses are more resilient or more integrated into host tissues. Such differences underscore adipose tissues, including PVAT, as dynamic microbial reservoirs, possibly shaped by its proximity to vascular beds and immune cells, including macrophages and T lymphocytes, which may foster selective microbial persistence.

Is there a PVAT-resident microbiome?

Microbial signatures are detectable across PVAT and non-PVAT depots and in feces in Dahl SS rats, but the structure and overlap of these communities differ between bacteria and viruses and across adipose tissue depots, and the time of collection influences these patterns.

PVAT contains a stromal vascular fraction enriched in immune cells, including macrophages and T lymphocytes [13,15,16]. PVAT is also known to modulate vascular tone [3,14,42], and microbial components could amplify this via immunomodulation or metabolite production [1,43]. Although the present study is descriptive and does not establish biological function, the detection of microbial signatures within PVAT raises the possibility that tissue-associated microbial components may interact with local immune and vascular pathways.

Bacterial communities exhibited a broader shared core in feces and more heterogeneous, tissue- and animal-specific patterns in PVAT and non-PVAT adipose tissues. In contrast, viral communities showed limited overlap, dominance by a few taxa, and minimal continuity with fecal profiles. These findings highlight the high spatial specificity and inter-individual variability of both bacterial and viral components of the microbiome in adipose-associated tissues and emphasize the value of analyzing PVAT as a distinct microenvironment rather than extrapolating from fecal data alone. Importantly, even when taxa were detected across multiple tissues, their relative abundances varied substantially, underscoring that presence alone does not imply uniform representation across compartments. Our work provides a foundational, descriptive framework for future studies aimed at exploring the biological relevance of tissue-associated microbiomes in cardiovascular and metabolic contexts, while underscoring the need for careful, compartment-specific interpretation.

Limitations:

The cohort-specific differences (2023 vs. 2024) raise questions about reproducibility (e.g., due to environmental factors, storage conditions, or laboratory procedures). While this is not a limitation in itself, the paper highlights it as a cornerstone that researchers must be mindful of when investigating the microbiome's influence. We share with you, transparently, our findings such that this issue of variability can be considered. Another limitation is the small sample size (n = 6 rats; 3 per cohort), which is common in microbiome studies and typically requires larger cohorts to achieve adequate statistical power. This may limit generalizability, and reliance on relative abundance metrics without absolute quantification or functional metagenomics. Although aseptic collection minimized contamination, environmental influences cannot be entirely excluded. The Dahl SS rat model, while relevant to vascular studies, may not fully translate to humans, in which PVAT composition varies.

5. Conclusions

PVAT from the Dahl SS rat harbors distinct bacteria and viruses, with bacterial composition showing cohort-specific temporal variability, unlike stable viral profiles. Non-PVAT and fecal samples exhibited lower overall variability than PVAT samples. Our analyses did not identify

 doi:10.20944/preprints202602.2014.v1

differences in microbiome composition between PVAT surrounding conductance vessels (thoracic and abdominal aorta) and resistance vessels (mesenteric arteries), neither significant clustering by PVAT depot in either bacterial or viral communities. Bray–Curtis ordination indicated that cohort (year of collection) and inter-individual variability had a stronger influence on community composition than anatomical location.

Temporal and environmental variables appear to exceed anatomical depot identity in structuring adipose-associated microbial communities. The greater dispersion observed in viral communities further suggests that the adipose virome may be more dynamically variable across sampling periods than the bacterial microbiome, although mechanistic drivers cannot be inferred from the present data.

As the first report of its kind, this study paves the way for investigating PVAT microbial roles in vascular homeostasis, immune modulation, and potential pharmacological targets for microbiome-based interventions in cardiovascular dysfunction. Future studies should incorporate larger cohorts, absolute quantification approaches, orthogonal validation methods, human tissues and disease models. Interventional strategies such as microbiome modulation, transplantation paradigms, and targeted pharmacological study designs are necessary to determine whether tissue-associated microbial signatures exert causal effects on vascular homeostasis or immune regulation.

Supplementary Materials: The following supporting information can be downloaded at the website of this paper posted on Preprints.org, *BACTERIA-TOTAL.exe* and *VIRUSES-TOTAL.exe.*

Author Contributions: CBR and SWW: conceived the project and coordinated manuscript production. CBR: coordinated manuscript production. CBR, SWW, and JT participated in data collection. CBR, SM, and CBB performed the statistical analysis and prepared the figures. CBR, SM, CBB, JT, and SWW contributed equally to writing the manuscript. CBR edited the final version. CBR, SM, JT, CBB, and SWW critically revised and approved the final manuscript. CBR, SM, CBB, JT, and SWW are responsible for the intellectual content of the final version.

Funding: Foundry for Innovative Research and Education Program at MSUCOM (#2025_PAT-FIRE_001) and NHLBI P01HL152951 funded this exploratory work.

Institutional Review Board Statement: All animal procedures were approved by the Michigan State University Institutional Animal Care and Use Committee (IACUC; PROTO202200001) and adhered to the *Guide for the Care and Use of Laboratory Animals* (8th edition, 2011) and ARRIVE guidelines.

Data Availability Statement: The original data presented in the study are openly available as supplementary material [Excel files named: *BACTERIA-TOTAL* and *VIRUSES-TOTAL*].

Acknowledgments: We thank Michigan State University College of Osteopathic Medicine (MSUCOM), the Foundry for Innovative Research and Education Program at MSUCOM, the Department of Pharmacology and Toxicology for providing academic support, and the NHLBI P01HL152951.

Conflicts of Interest: The authors declare no relevant financial or non-financial interests.

References

1. Agabiti-Rosei C, Saxton SN, De Ciuceis C, Lorenza Muiesan M, Rizzoni D, Agabiti Rosei E, et al. Influence of Perivascular Adipose Tissue on Microcirculation: A Link Between Hypertension and Obesity. Hypertension. Ovid Technologies (Wolters Kluwer Health); 2024;81:24–33. https://doi.org/10.1161/hypertensionaha.123.19437
2. Chang L, Garcia-Barrio MT, Chen YE. Perivascular Adipose Tissue Regulates Vascular Function by Targeting Vascular Smooth Muscle Cells. ATVB. Ovid Technologies (Wolters Kluwer Health); 2020;40:1094–109. https://doi.org/10.1161/atvbaha.120.312464

 doi:10.20944/preprints202602.2014.v1

3. Soltis EE, Cassis LA. Influence of Perivascular Adipose Tissue on Rat Aortic Smooth Muscle Responsiveness. Clinical and Experimental Hypertension Part A: Theory and Practice. Informa UK Limited; 1991;13:277–96. https://doi.org/10.3109/10641969109042063
4. Withers SB, Forman R, Meza-Perez S, Sorobetea D, Sitnik K, Hopwood T, et al. Eosinophils are key regulators of perivascular adipose tissue and vascular functionality. Sci Rep [Internet]. Springer Science and Business Media LLC; 2017 [cited 2025 July 19];7. https://doi.org/10.1038/srep44571
5. Ayala-Lopez N, Martini M, Jackson WF, Darios E, Burnett R, Seitz B, et al. Perivascular adipose tissue contains functional catecholamines. Pharmacology Res & Perspec [Internet]. Wiley; 2014 [cited 2025 July 19];2. https://doi.org/10.1002/prp2.41
6. Gao Y-J, Zeng Z, Teoh K, Sharma AM, Abouzahr L, Cybulsky I, et al. Perivascular adipose tissue modulates vascular function in the human internal thoracic artery. The Journal of Thoracic and Cardiovascular Surgery. Elsevier BV; 2005;130:1130–6. https://doi.org/10.1016/j.jtcvs.2005.05.028
7. Thompson JM, Watts SW, Terrian L, Contreras GA, Rockwell C, Rendon CJ, et al. A cell atlas of thoracic aortic perivascular adipose tissue: a focus on mechanotransducers. American Journal of Physiology-Heart and Circulatory Physiology. American Physiological Society; 2024;326:H1252–65. https://doi.org/10.1152/ajpheart.00040.2024
8. Restini CBA, Ismail A, Kumar RK, Burnett R, Garver H, Fink GD, et al. Renal perivascular adipose tissue: Form and function. Vascular Pharmacology. Elsevier BV; 2018;106:37–45. https://doi.org/10.1016/j.vph.2018.02.004
9. Lin A, Dey D, Wong DTL, Nerlekar N. Perivascular Adipose Tissue and Coronary Atherosclerosis: from Biology to Imaging Phenotyping. Curr Atheroscler Rep [Internet]. Springer Science and Business Media LLC; 2019 [cited 2025 July 19];21. https://doi.org/10.1007/s11883-019-0817-3
10. Verlohren S, Dubrovska G, Tsang S-Y, Essin K, Luft FC, Huang Y, et al. Visceral Periadventitial Adipose Tissue Regulates Arterial Tone of Mesenteric Arteries. Hypertension. Ovid Technologies (Wolters Kluwer Health); 2004;44:271–6. https://doi.org/10.1161/01.hyp.0000140058.28994.ec
11. Keane J, Longhi MP. Perivascular Adipose Tissue Niches for Modulating Immune Cell Function. ATVB. Ovid Technologies (Wolters Kluwer Health); 2025;45:857–65. https://doi.org/10.1161/atvbaha.124.321696
12. Kruit N, Sluiter TJ, De Vries MR. Role of Perivascular Adipose Tissue in Vein Remodeling. ATVB. Ovid Technologies (Wolters Kluwer Health); 2025;45:576–84. https://doi.org/10.1161/atvbaha.124.321692
13. Kumar RK, Yang Y, Contreras AG, Garver H, Bhattacharya S, Fink GD, et al. Phenotypic Changes in T Cell and Macrophage Subtypes in Perivascular Adipose Tissues Precede High-Fat Diet-Induced Hypertension. Front Physiol [Internet]. Frontiers Media SA; 2021 [cited 2025 July 19];12. https://doi.org/10.3389/fphys.2021.616055
14. Watts SW, Flood ED, Garver H, Fink GD, Roccabianca S. A New Function for Perivascular Adipose Tissue (PVAT): Assistance of Arterial Stress Relaxation. Sci Rep [Internet]. Springer Science and Business Media LLC; 2020 [cited 2025 July 19];10. https://doi.org/10.1038/s41598-020-58368-x
15. Kumar RK, Jin Y, Watts SW, Rockwell CE. Naïve, Regulatory, Activated, and Memory Immune Cells Co-exist in PVATs That Are Comparable in Density to Non-PVAT Fats in Health. Front Physiol [Internet]. Frontiers Media SA; 2020 [cited 2025 July 19];11. https://doi.org/10.3389/fphys.2020.00058
16. Jin Y, Liu S, Guzmán KE, Kumar RK, Kaiser LM, Garver H, et al. PVAT-conditioned media from Dahl S rats on high fat diet promotes inflammatory cytokine secretion by activated T cells prior to the development of hypertension. Wang J, editor. PLoS ONE. Public Library of Science (PLoS); 2024;19:e0302503. https://doi.org/10.1371/journal.pone.0302503
17. Hillock-Watling C, Gotlieb AI. The pathobiology of perivascular adipose tissue (PVAT), the fourth layer of the blood vessel wall. Cardiovascular Pathology. Elsevier BV; 2022;61:107459. https://doi.org/10.1016/j.carpath.2022.107459
18. Huang Cao ZF, Stoffel E, Cohen P. Role of Perivascular Adipose Tissue in Vascular Physiology and Pathology. Hypertension. Ovid Technologies (Wolters Kluwer Health); 2017;69:770–7. https://doi.org/10.1161/hypertensionaha.116.08451

 doi:10.20944/preprints202602.2014.v1

19. Queiroz M, Sena CM. Perivascular adipose tissue: a central player in the triad of diabetes, obesity, and cardiovascular health. Cardiovasc Diabetol [Internet]. Springer Science and Business Media LLC; 2024 [cited 2025 July 19];23. https://doi.org/10.1186/s12933-024-02549-9
20. Massier L, Chakaroun R, Tabei S, Crane A, Didt KD, Fallmann J, et al. Adipose tissue derived bacteria are associated with inflammation in obesity and type 2 diabetes. Gut. BMJ; 2020;69:1796–806. https://doi.org/10.1136/gutjnl-2019-320118
21. Belkaid Y, Hand TW. Role of the Microbiota in Immunity and Inflammation. Cell. Elsevier BV; 2014;157:121–41. https://doi.org/10.1016/j.cell.2014.03.011
22. Yang T, Mei X, Tackie-Yarboi E, Akere MT, Kyoung J, Mell B, et al. Identification of a Gut Commensal That Compromises the Blood Pressure-Lowering Effect of Ester Angiotensin-Converting Enzyme Inhibitors. Hypertension. Ovid Technologies (Wolters Kluwer Health); 2022;79:1591–601. https://doi.org/10.1161/hypertensionaha.121.18711
23. Yang T, Maki KA, Marques FZ, Cai J, Joe B, Pepine CJ, et al. Hypertension and the Gut Microbiome: A Science Advisory From the American Heart Association. Hypertension. 2025; https://doi.org/10.1161/HYP.0000000000000247
24. Wang C, Yi Z, Jiao Y, Shen Z, Yang F, Zhu S. Gut Microbiota and Adipose Tissue Microenvironment Interactions in Obesity. Metabolites. 2023;13:821. https://doi.org/10.3390/metabo13070821
25. Rapp JP, Dene H. Development and characteristics of inbred strains of Dahl salt-sensitive and salt-resistant rats. Hypertension. 1985;7:340–9.
26. Spradley FT, Ho DH, Pollock JS. Dahl SS rats demonstrate enhanced aortic perivascular adipose tissue-mediated buffering of vasoconstriction through activation of NOS in the endothelium. American Journal of Physiology-Regulatory, Integrative and Comparative Physiology. American Physiological Society; 2016;310:R286–96. https://doi.org/10.1152/ajpregu.00469.2014
27. Watts SW, Darios ES, Contreras GA, Garver H, Fink GD. Male and female high-fat diet-fed Dahl SS rats are largely protected from vascular dysfunctions: PVAT contributions reveal sex differences. American Journal of Physiology-Heart and Circulatory Physiology. 2021;321:H15–28. https://doi.org/10.1152/ajpheart.00131.2021
28. Li H, Durbin R. Fast and accurate short read alignment with Burrows–Wheeler transform. Bioinformatics. 2009;25:1754–60. https://doi.org/10.1093/bioinformatics/btp324
29. Oksanen J, Simpson GL, Blanchet FG, Kindt R, Legendre P, Minchin PR, et al. vegan: Community Ecology Package [Internet]. 2001 [cited 2026 Jan 2]. p. 2.7-2. https://doi.org/10.32614/CRAN.package.vegan
30. Legendre P, De Cáceres M. Beta diversity as the variance of community data: dissimilarity coefficients and partitioning. Morlon H, editor. Ecology Letters. 2013;16:951–63. https://doi.org/10.1111/ele.12141
31. Anderson MJ. Distance-Based Tests for Homogeneity of Multivariate Dispersions. Biometrics. 2006;62:245–53. https://doi.org/10.1111/j.1541-0420.2005.00440.x
32. Ahmadieh S, Kim HW, Weintraub NL. Potential role of perivascular adipose tissue in modulating atherosclerosis. Clinical Science. 2020;134:3–13. https://doi.org/10.1042/CS20190577
33. Salter SJ, Cox MJ, Turek EM, Calus ST, Cookson WO, Moffatt MF, et al. Reagent and laboratory contamination can critically impact sequence-based microbiome analyses. BMC Biol. 2014;12:87. https://doi.org/10.1186/s12915-014-0087-z
34. Wulczynski M, Brooks SPJ, Green J, Matias F, Kalmokoff M, Green-Johnson JM, et al. Environmental enrichment with nylon gnaw sticks introduces variation in Sprague Dawley rat immune and lower gastrointestinal parameters with differences between sexes. anim microbiome. 2025;7:12. https://doi.org/10.1186/s42523-024-00369-6
35. Patel D, Sharma D, Mandal P. Gut Microbiota: Target for Modulation of Gut-Liver-Adipose Tissue Axis in Ethanol-Induced Liver Disease. Pritchard MT, editor. Mediators of Inflammation. 2022;2022:1–11. https://doi.org/10.1155/2022/4230599
36. Queiroz M, Sena CM. Perivascular adipose tissue: a central player in the triad of diabetes, obesity, and cardiovascular health. Cardiovasc Diabetol. 2024;23:455. https://doi.org/10.1186/s12933-024-02549-9

 doi:10.20944/preprints202602.2014.v1

37. Wilcox CS, Herbert C, Wang C, Ma Y, Sun P, Li T, et al. Signals From Inflamed Perivascular Adipose Tissue Contribute to Small-Vessel Dysfunction in Women With Human Immunodeficiency Virus. The Journal of Infectious Diseases. 2024;230:67–77. https://doi.org/10.1093/infdis/jiae094
38. Zhang S, Jiang J, Luo Y, Liu G, Hu S, Wan S, et al. Molecular crosstalk in perivascular adipose tissue: mechanisms of inflammation, metabolic dysregulation, and therapeutic opportunities in cardiovascular disease. Front Cardiovasc Med. 2025;12:1613900. https://doi.org/10.3389/fcvm.2025.1613900
39. Dwaib HS, AlZaim I, Ajouz G, Eid AH, El-Yazbi A. Sex Differences in Cardiovascular Impact of Early Metabolic Impairment: Interplay between Dysbiosis and Adipose Inflammation. Molecular Pharmacology. 2022;102:60–79. https://doi.org/10.1124/molpharm.121.000338
40. Restini CBA, Fink GD, Watts SW. Vascular reactivity stimulated by TMA and TMAO: Are perivascular adipose tissue and endothelium involved? Pharmacological Research. Elsevier BV; 2021;163:105273. https://doi.org/10.1016/j.phrs.2020.105273
41. Shen J, Obin MS, Zhao L. The gut microbiota, obesity and insulin resistance. Molecular Aspects of Medicine. 2013;34:39–58. https://doi.org/10.1016/j.mam.2012.11.001
42. Schroeter MR, Eschholz N, Herzberg S, Jerchel I, Leifheit-Nestler M, Czepluch FS, et al. Leptin-Dependent and Leptin-Independent Paracrine Effects of Perivascular Adipose Tissue on Neointima Formation. ATVB. 2013;33:980–7. https://doi.org/10.1161/ATVBAHA.113.301393
43. Saxton SN, Clark BJ, Withers SB, Eringa EC, Heagerty AM. Mechanistic Links Between Obesity, Diabetes, and Blood Pressure: Role of Perivascular Adipose Tissue. Physiological Reviews. 2019;99:1701–63. https://doi.org/10.1152/physrev.00034.2018